Environ. Sci. Technol. **2008,** *42,* 1766–1772

Formation of Metallic Copper Nanoparticles at the Soil–Root Interface

ALAIN MANCEAU,*,† KATHRYN L. NAGY,‡ MATTHEW A. MARCUS,§ MARTINE LANSON,† NICOLAS GEOFFROY,† THIERRY JACQUET,△ AND TATIANA KIRPICHTCHIKOVA△

LGIT-Maison des Géosciences, CNRS and Université J. Fourier, 38041 Grenoble Cedex 9, France, Department of Earth and Environmental Sciences, 845 West Taylor Street, MC-186, University of Illinois at Chicago, Chicago, Illinois 60607, Advanced Light Source, Lawrence Berkeley National Laboratory, One Cyclotron Road, Berkeley, California 94720, and Phytorestore—Site et Concept, Hôtel Vigée Le Brun, 8 rue du Sentier, 75002 Paris, France

Received August 13, 2007. Revised manuscript received November 16, 2007. Accepted December 10, 2007.

Copper is an essential element in the cellular electron-transport chain, but as a free ion it can catalyze production of damaging radicals. Thus, all life forms attempt to prevent copper toxicity. Plants diminish excess copper in two structural regions: rare hyperaccumulators bind cationic copper to organic ligands in subaerial tissues, whereas widespread metal-tolerant plants segregate copper dominantly in roots by mechanisms thought to be analogous. Here we show using synchrotron microanalyses that common wetlands plants *Phragmites australis* and *Iris pseudoacorus* can transform copper into metallic nanoparticles in and near roots with evidence of assistance by endomycorrhizal fungi when grown in contaminated soil in the natural environment. Biomolecular responses to oxidative stress, similar to reactions used to abiotically synthesize Cu^0 nanostructures of controlled size and shape, likely cause the transformation. This newly identified mode of copper biomineralization by plant roots under copper stress may be common in oxygenated environments.

Introduction

Copper is toxic to life at levels that vary depending on the organism. Humans are mandated to not exceed 1–2 mg/L copper in their drinking water (*1, 2*), while some freshwater animals and plants experience acute toxic effects at concentrations as low as 10 μg/L (*3*). Because the human food chain begins with plants, it is critical to understand how plants tolerate heavy metals including copper, which is frequently concentrated in soils as a result of pesticide application, sewage sludge deposition, mining, smeltering, and industrial activities. This issue is also at the crux of applying phytoremediation approaches, which use green plants to decontaminate or contain polluted soils and sediments and to purify wastewaters and landfill leachates (*4*).

Metal-tolerant plants inhibit incorporation of excess metal into photosynthetic tissue by restricting transport across the root endodermis (stele) and by storage in the root cortex (*5*). In contrast, hyperaccumulating plants extract metals from soils and concentrate excess amounts in harvestable parts such as leaves. Copper detoxification seems to be linked to mechanisms that bind Cu to molecular thiol (SH) groups. Cysteine-rich peptides, such as phytochelatins which transport copper to the shoot, increase in response to high cellular levels of Cu (*6, 7*), and Cu–S binding occurs in roots and leaves of *Larrea tridentata* (Creosote bush) (*8*). However, an unidentified copper species, concentrated in electron-dense granules on cell walls and some vacuole membranes, appears to be the main morphological form of copper sequestered in *Oryza sativa* (rice), *Cannabis sativa* (marijuana), *Allium sativum* (garlic), and *Astragalus sinicus* (Chinese milk vetch) (*9–12*).

Plants take in and exclude elements largely at the soil–root interface within the rhizosphere, i.e. the volume of soil influenced by roots, mycorrhizal fungi, and bacterial communities (*13*). Deciphering processes that control the bioavailability of metals in the field is difficult because the rhizosphere is compositionally and structurally complex. Here we report on using synchrotron-based microanalytical and imaging tools (*14*) to resolve processes by which metal-tolerant plants defend themselves against excess cationic copper. We have mapped the distribution of copper in self-standing thin sections of unperturbed soils using micro-X-ray fluorescence (μ-XRF) and identified structural forms of copper at points-of-interest (POIs) using micro-extended X-ray absorption fine structure (μ-EXAFS) spectroscopy and X-ray diffraction (μ-XRD). Because only a few small areas could be analyzed in reasonable times with microanalyses, the uniqueness of the microanalytical results was tested by recording the bulk EXAFS spectrum from a sample representing the entire rhizosphere and by simulating this spectrum by linear combination of copper species spectra from POIs.

We investigated copper speciation in rhizospheres of *Phragmites australis* (common reed) and *Iris pseudoacorus*, two widespread wetland species with high tolerances to heavy metals (*15*). *P. australis* is frequently used to treat wastewaters (*16*) because it can store heavy metals as weakly soluble or insoluble forms. Its roots can be enriched in Cu 5–60 times relative to leaves, with large differences among ecotypes and between field-grown versus hydroponically grown plants (*17, 18*). To take into account natural complexity, including any influence of bacteria, fungi, or climate variation, our experiment was conducted outdoors, rather than in a greenhouse on seedlings using ex-solum pots or hydroponic growth methods. The soil was from the Pierrelaye plain, a 1200 ha truck-farming area about 30 km northwest of Paris, France. From 1899 to 1999, regular irrigation of the Pierrelaye plain with untreated sewage water from Paris caused contamination with heavy metals, mainly Zn, Pb, and Cu (*19*). Such pollution is pervasive worldwide because increasing populations and associated economic growth are diminishing available freshwater, thus leading to increased irrigation of farmlands with wastewaters.

Experimental Methods

Field Experiment. A detailed description of the phytoremediation experiment is given in Supporting Information.

* Corresponding author e-mail: manceau@obs.ujf-grenoble.fr.
† LGIT-Maison des Géosciences.
‡ University of Illinois at Chicago.
§ Lawrence Berkeley National Laboratory.
△ Phytorestore—Site et Concept.

10.1021/es072017o CCC: $40.75

Published on Web 01/26/2008

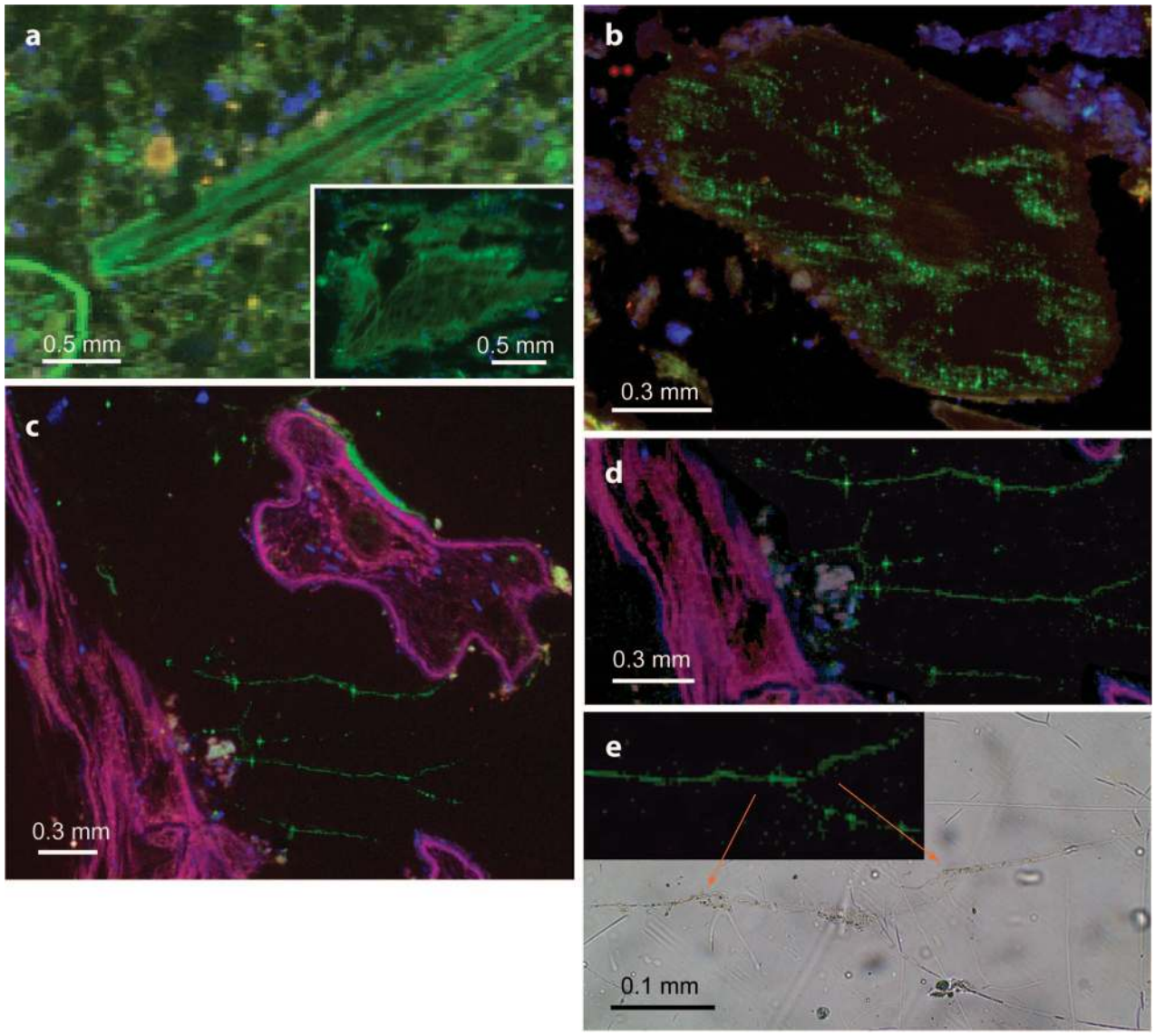

FIGURE 1. Micro-X-ray fluorescence (μ-XRF) maps showing the distribution of Zn (red), Cu (green), and Ca (blue) in the initial soil (a) and rhizospheres of *Phragmites australis* (b) and *Iris pseudoacorus* (c−e). (a) Green features are organic matter (resolution = 20 × 20 μm^2). The inset shows a reticular structure mapped at high resolution (9 × 9 μm^2). (b) Transversal section of a root with aggregates of Cu metal nanoparticles in the cortical region (resolution = 4 × 4 μm^2). The central stele region contains Zn but no Cu. (c) Although Zn occurs in the main roots of *I. pseudoacorus*, Cu is located in ramified organic filaments typical of mycorrhizal fungi and in a biofilm at the surface of the root (resolution = 8 × 8 μm^2). (d) Enlargement of the region rich in organic filaments showing two anastomosed hyphae. (e) Optical micrograph of one anastomosed hypha from panel d with fluorescence map in inset. Data collected on beamline 10.3.2 of the Advanced Light Source (ALS) at Lawrence Berkeley National Laboratory (*62*).

X-ray Fluorescence. Elemental distributions in the initial soil and rhizospheric soils vegetated with *P. australis* and *I. pseudoacorus* were mapped by scanning several 30-μm-thick thin sections under a 10.0 keV (vegetated soil) or 13.05 keV (unvegetated soil) micro-X-ray beam while recording the X-ray fluorescence. The soil is rich in organic debris from past agricultural activity which causes it to be optically inhomogeneous over a few to several hundreds of micrometers. Therefore, both coarse and fine μ-XRF maps were recorded at resolutions from 35 × 35 μm^2 to 4 × 4 μm^2 using a beam dimension adjusted from 16 (H) × 10 (V) μm^2 to 5 (H) × 5 (V) μm^2 to match the step size. The counting time per pixel was 100 ms at 10.0 keV and 200 ms at 13.05 keV. The scanning speed was fast enough to prevent alteration of the initial Cu speciation by beam damage.

EXAFS Spectroscopy. In the μ-EXAFS measurement, the organically bound Cu species evolved over 30−45 min due to the instability of organic matter to intense X-ray radiation. Radiation damage was minimized by reducing scan times to 20 min per analyzed area and moving the sample by 15 μm along the direction of an organic particle to access fresh material for every scan. Caution was taken that all individual spectra averaged out before summing to improve statistics. For bulk EXAFS measurements, samples were frozen at 10 K. All spectra were recorded in fluorescence-yield detection mode, except those from the Cu grains (μ-EXAFS), which were recorded in transmission mode.

X-ray Diffraction. Diffraction patterns were recorded in transmission mode with a Bruker 6000 CCD binned to 1024 × 1024 pixels.

Results and Interpretations

X-ray Fluorescence. In the initial soil, copper occurs in two morphological forms (Figure 1a). One form decorates coarse organic particles that have some recognizable structures from reticular tissue (insert in Figure 1a), and the other occurs in

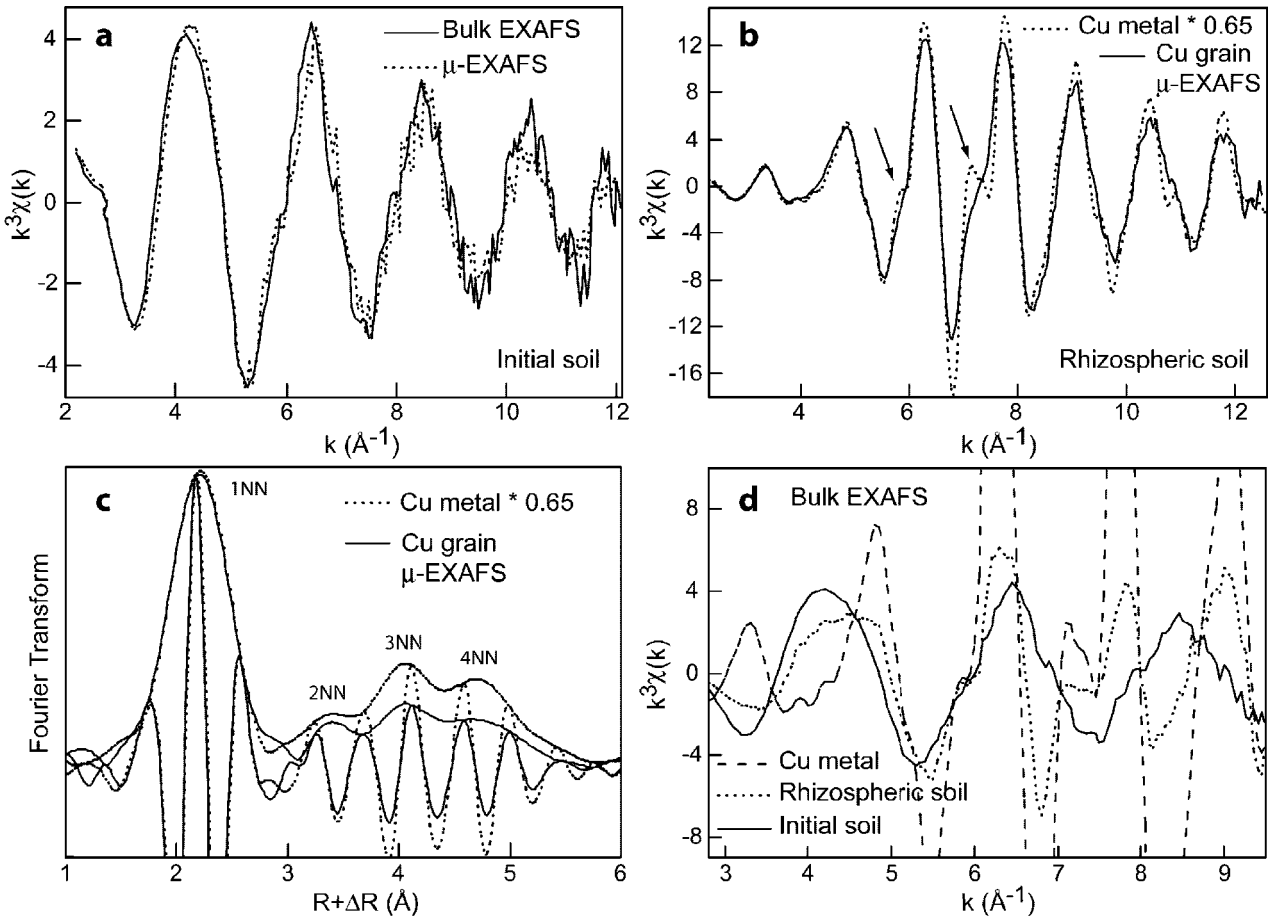

FIGURE 2. EXAFS data. (a) Representative Cu K-edge μ-EXAFS spectrum at room temperature of organic debris (dotted line) from the map in Figure 1a and the bulk EXAFS spectrum at 10 K of the initial soil (solid line). (b) Representative μ-EXAFS spectrum of Cu grains from *P. australis* rhizosphere (solid line) and bulk EXAFS spectrum of reference Cu metal at room temperature. The amplitude of the reference spectrum was multiplied by 0.65. (c) Fourier transform (modulus plus imaginary part) of the EXAFS spectra in panel b. The amplitude of the reference's first shell peak (1NN contribution) was scaled to that of the sample by multiplying the reference EXAFS signal by 0.65. (d) Bulk EXAFS spectra of the initial soil (10 K, solid line), *P. australis* rhizosphere (10 K, dotted line), and Cu metal (room temperature, dashed line). The spectrum for the *I. pseudoacorus* rhizosphere is similar to that of *P. australis* and was omitted for clarity. The μ-EXAFS data were recorded on beamline 10.3.2 at the ALS and the bulk EXAFS data on the FAME beamline (BM 30B) at the European Synchrotron Radiation Facility (ESRF, France) (*63*).

the fine clayey matrix in areas that show organic particulate shapes only at high μ-XRF resolution. In the two phytoremediated soils, similar Cu−organic particulate associations, but also, hot spots of Cu grains 5−20 μm in size were observed in the thin-section maps (Figure 1b−d). In the rhizosphere of *P. australis*, the Cu hot spots exist outside and in roots and specifically in cortical parenchyma, but not in central vascular cylinders from the stele that contain vascular bundles through which micronutrients are transported to reproductive and photosynthetic tissues. In contrast, the main roots and rhizome of *I. pseudoacorus* do not contain detectable Cu grains, but in the surrounding soil Cu grains are aligned, suggesting that they are associated with biological structures. Under an optical microscope filamentous and ramified organic structures, similar to root hairs or hyphae from endomycorrhizal fungi, are visible in places where the Cu spots were observed by μ-XRF (Figure 1e, Supporting Information). Fungal forms are more likely because mycorrhizal hyphae typically are anastomosing, whereas root hairs are not. Fungi may also be implicated in the formation of Cu grains in the cortex of *P. australis* since roots of this plant are known to be colonized by arbuscular endomycorrhizae in contaminated environments (*20*). These hypotheses are consistent with the capacity of mycorrhizae to accumulate metals (*21–23*) and with the storage of Cu in secondary feeder roots of the water hyacinth *Eichhornia crassipes* (*24*). The Cu grains have about the same size as the electron-dense Cu granules (~2 μm) in cells of *E. splendens* placed in a $CuSO_4$ solution for 30 days (*12*).

EXAFS Spectroscopy. *Organic Cu.* While biological activity clearly modified the original distribution of Cu in the rhizospheres, the Cu species could not be identified from the μ-XRF maps but instead were elucidated using EXAFS spectroscopy. All eight μ-EXAFS spectra from areas in the original soil containing the particle morphologies and chemical compositions observed with μ-XRF can be superimposed on the soil's bulk EXAFS spectrum (Figure 2a), indicating that the initial Cu speciation occurred uniformly. If the initial soil contained various assemblages of Cu species that were distributed unevenly, then we might expect that the proportions of species also would have varied among analyzed areas and been detectable by μ-EXAFS spectroscopy (*25*); however, this was not observed. These spectra match those for Cu^{2+} binding to carboxyl ligands in natural organic matter, as commonly observed (Supporting Information).

Elemental Cu. In contrast, only the reference spectrum of elemental copper (Cu^0) matches the μ-EXAFS spectra of the 12 hot-spot Cu grains, which are statistically invariant (Figure 2b, Supporting Information). Photoreduction of Cu^{2+} in the X-ray beam cannot explain the formation of Cu^0 because (i) no elemental Cu was detected in the initial soil by powder and μ-EXAFS, and (ii) Cu^0 was detected in the two phytore-

mediated soils at 10 K by bulk EXAFS, and all individual spectral scans from the same sample could be superimposed. At 10 K, radiation damage is delayed (*14*), and if Cu had been reduced in the beam, the proportion of Cu^0 would have increased from scan to scan which was not observed.

Spectra for rhizosphere Cu grains and reference metallic copper have the same phase and overall line shape, but they have significant differences in fine structure and amplitude, which provide details about the nature of the Cu grains. In the soil Cu grains, shoulders at 5.8 and 7.3 $Å^{-1}$ are weak and the spectral amplitude is reduced by about 35% and attenuated, relative to metallic copper. The decreased amplitude of the EXAFS signal for the Cu grains relative to well-crystallized metallic copper cannot arise from overabsorption (*14*) because the spectra of the grains were recorded in transmission mode and because the amplitude reduction from overabsorption would be uniform in *R*-space, as demonstrated for ZnS and MnO_2 particles (*26, 27*), which does not occur in this case.

Derived radial structure–functions share the four-peak character of Cu metal (*28*) (Figure 2c). However, long-distance pair correlations (i.e., the high-frequency components in *k* space) are progressively diminished in the soil spectra, indicating multiple interatomic distances (structural disorder), reduced coordination numbers (CNs) from small particles (size effect), and/or abundant microstructural defects, such as grain and twin boundary dislocations or atomic-scale vacancies.

Simulation of the data using multiple-scattering ab initio FEFF calculations showed no evidence for structural disorder (Supporting Information). Good agreement between calculated and observed spectra was obtained with a first nearest-neighbor shell (1NN) of 7.8 Cu atoms at 2.55 Å, a second shell (2NN) of 2.7 Cu at 3.61 Å, a third shell (3NN) of 9.2 Cu at 4.43 Å, and a fourth shell (4NN) of 3.9 Cu at 5.11 Å, compared to 1NN of 12 at 2.55 Å, 2NN of 6 at 3.61 Å, 3NN of 24 at 4.43 Å, and 4NN of 12 at 5.11 Å, in crystalline Cu metal. The mean-square displacement of bond length parameter (σ^2), a measure of disorder, converged in the simulated spectra to the same value as in the Cu metal reference (0.01 $Å^2$) showing that Cu−Cu bonds vary in length by the same amount in the soil grains and reference.

Although the rhizosphere Cu grains are not structurally disordered, their CNs are only 65% (1NN), 45% (2NN), 38% (3NN), and 32% (4NN) of those in the Cu metal spectrum, indicating that structural order is limited in extent. The lower CN values are consistent with small particles having incompletely coordinated surface atoms. If closed-shell packed and monodispersed, these particles would have a minimum size of 10–15 Å assuming a spherical cuboctahedron shape and 15–20 Å assuming a hemispherical shape, as reported for nanoscale platinum particles (*29*). If Cu atoms were missing (e.g., atomic vacancies), as reported for Fe metal powders with a first-shell CN reduced by up to 50% of that in metallic Fe, the effective particle size could be as high as ca. 100 Å in diameter (*30*). A defective nanoparticle model is appealing because the surface area-to-volume ratio increases with only a lattice-vacancy parameter.

Constitutive nanoparticles in the micrometer-sized Cu grains are joined at particle or so-called grain boundaries, which might contain stabilizing organic molecules. Complexation of Cu to sulfur ligands in the interparticle or surficial regions is unlikely because a low-*R* Fourier component from Cu−S pairs at 2.2–2.3 Å was not observed on the radial structure–function (*8*). Also, the first Cu−Cu distance of 2.56 Å in the Cu nanoparticle is shorter than the distance of 2.70–2.90 Å reported for Cu−thiolate clusters (*8, 31*) and matches only that in elemental copper. In addition, organic S or P was not observed in the Cu grains using scanning electron microscopy−energy dispersive X-ray fluorescence (SEM-EDX) in agreement with observations on electron-dense Cu granules in plants using electron energy loss spectroscopy (EELS) and EDX (*10, 12*). Complexation to oxygen ligands is possible because EXAFS has relatively low sensitivity to low-Z atoms. However, linear combinations of experimental spectra for organically bound Cu^{2+} and nanometallic Cu show that the fraction of potential organic Cu in the Cu grains is less than 15%, if present at all (Supporting Information).

Amounts of Organic and Elemental Cu in the Rhizospheres. Composite bulk EXAFS spectra of the two remediated soils and spectra from the two species identified by μ-EXAFS (Figure 2d) intersect at the same *k* values, confirming that only two main Cu species exist in both rhizospheres. Fractional amounts of organically bound Cu from the original soil and metallic Cu formed during phytoremediation were estimated by reconstructing the bulk spectra with linear combinations of the two single species spectra. The best fit for the rhizosphere of *P. australis* was obtained with 75 ± 10% organic-bound Cu^{2+} and 25 ± 10% Cu^0. The rhizosphere of *I. pseudoacorus* contains slightly less Cu^0 (20 ± 10%).

X-ray Diffraction. Featureless two-dimensional μ-XRD patterns from eight Cu hot spots confirm that the Cu grains are aggregates of nanoparticles. However, three patterns display a faint continuous diffraction ring at the Bragg angle for the brightest 111 reflection of Cu metal, indicating larger individual particles with a domain size of 130–150 Å (Figure 3). About 25×10^4 larger particles would be needed to produce these XRD patterns, but they would comprise only about 0.01% of the analyzed volume (Supporting Information). Thus, the diffracting Cu hot spots may have sufficient big particles to yield a powder ring, but they are not enough for their 2NN, 3NN, and higher Cu-Cu shells to contribute significantly to the EXAFS signal. Also, the big particles are undetected by μ-EXAFS because EXAFS signal intensity is linearly proportional to the number of atoms whereas XRD intensity is proportional to the number of atoms squared.

Discussion

Mechanism of Cu^{2+} to Cu^0 Reduction. The rhizospheres were oxidizing as indicated by the presence of iron oxyhydroxide (goethite), absence of sulfide minerals, and the fact that *P. australis* and *I. pseudoacorus* are typical wetlands plants with aerenchyma that facilitate oxygen flow from leaves to roots (*32*). Thermodynamic calculations using compositions of soil solutions collected below the rhizosphere indicate that Cu^+ and Cu^{2+} species should have been dominant (Supporting Information). These points along with the occurrences of nanocrystalline Cu^0 in plant cortical cells and as stringer morphologies outside the roots together suggest that copper was reduced biotically. Ecosystem ecology of the rhizosphere indicates synergistic or multiple reactions by three types of organisms: plants, endomycorrhizal fungi, and bacteria.

Normally, organisms maintain copper homeostasis through cation binding to bioactive molecules such as proteins and peptides. When bound, the Cu^{2+}/Cu^{1+} redox couple has elevated half-cell potentials (*33*) that facilitate reactions in the electron-transport chain. Even though average healthy cell environments are sufficiently reducing (*34*), there are enough binding sites (*35*) to maintain copper in its two oxidized states. Copper is also important in controlling cell-damaging free radicals produced at the end of the electron-transport chain, for example in the superoxide dismutase enzyme Cu-Zn-SOD, which accelerates the disproportionation of superoxide to O_2 and hydrogen peroxide. However, unbound copper ions can catalyze the decomposition of hydrogen peroxide to water and more free radical species. To combat toxic copper and free radicals, many organisms overproduce enzymes such as catalase, chelates such as glutathione, and antioxidants (*36*). Mineralization

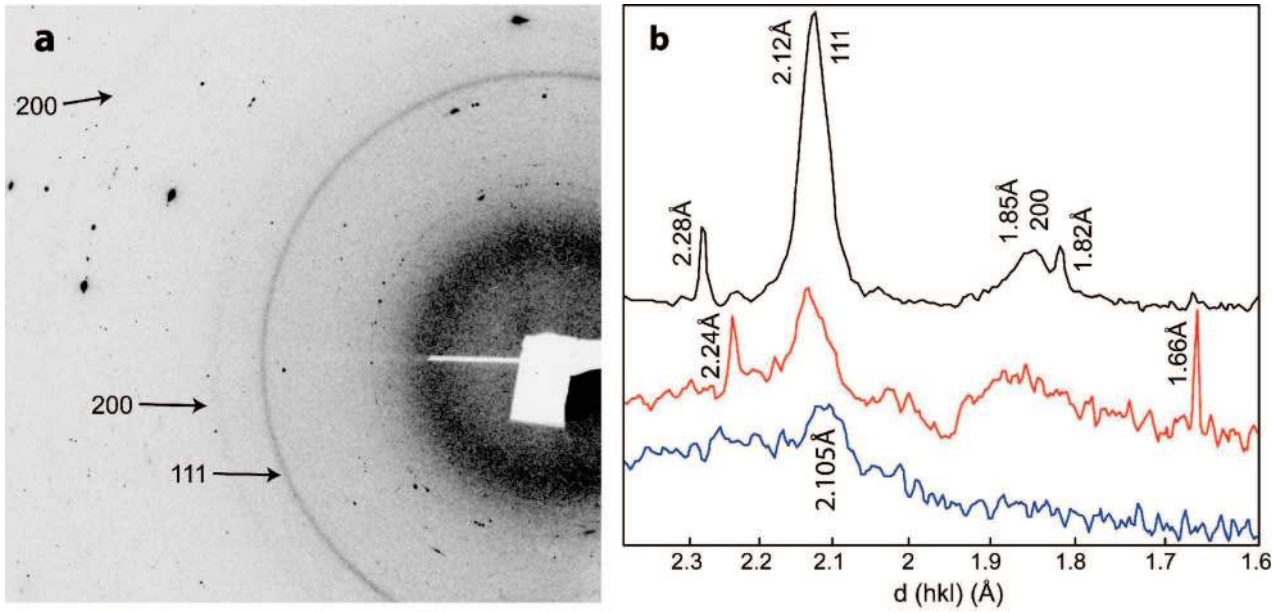

FIGURE 3. XRD data. (a) Two-dimensional μ-XRD pattern of a Cu grain showing the 111, 200, and 220 reflections of Cu metal. The spotty reflections are from coarse quartz grains (d = 2.28, 2.24, 1.82, 1.66 Å), and were used as internal calibration standards. (b) One-dimensional patterns obtained by summing intensities radially at constant Bragg angle. The pattern in black is from the Cu grain whose 2D pattern is shown in panel a. The two other patterns are from different grains. Their 111 reflections are too faint to be viewed on the 2D image, and they can be observed only after integration. The d(111) and d(200) spacings are shifted by +0.015 to +0.04 Å relative to pure Cu^0 (d(111) = 2.09 Å and d(200) = 1.81 Å), due probably to the incorporation of trace elements (e.g., Sn, W, Zn), as commonly observed in metallic copper. Recording conditions: energy = 17 keV, beam size = 16 (H) × 7 (V) μm^2, exposure time = 120 s.

could also be a defense against toxic copper, but reports of Cu^+ and Cu^{2+} biominerals are rare; only copper sulfide in yeast (*37*) and copper oxalate in lichens (*38*) and fungi (*23*) are known. Atacamite ($Cu_2(OH)_3Cl$) in worms (*39*) does not appear to result from a biochemical defense.

Biomineralization of copper metal may have occurred by a mechanism analogous to processes for metallic nanoparticle synthesis that exploit ligand properties of organic molecules. In these processes, organic molecules are used as templates to control the shape and size of metallic nanoparticles (*40, 41*) formed by adding strong reductants to bound cations. For copper nanoparticles and nanowires, a milder reductant—ascorbic acid—has been used. Ascorbic acid, a well-known antioxidant, reduces Cu cations to Cu^0 only when the cations are bound to organic substrates such as DNA in the presence of oxygen in the dark (*42*) or via autocatalysis on Cu metal seeds in the absence of stabilizing organic ligands (*43*). As an example of synthetic control, pH-dependent conformation of histidine-rich peptides has led to larger nanocrystals of Cu^0 at pH 7–10 than at pH 4–6 (*44*).

Plants produce ascorbic acid for many functions (*45*) and rhizospheres often contain the breakdown products of ascorbic acid, which facilitates electron transfer during mineral weathering (*46*). Plants produce more ascorbic acid when grown in soils contaminated with heavy metals including copper (*47*). Fungi, which proliferate over plants (*48*) and bacteria (*23*) in metal-contaminated soils, can stabilize excess copper (*49*) by extracellular cation binding or oxalate precipitation (*23*), but mechanisms probably also require enzymes, thiol-rich proteins and peptides, and antioxidants (*23, 48, 50*). The formation of electron-dense Cu granules within hyphae of arbuscular mycorrhizal fungi isolated from Cu- and As-contaminated soil (*51*) suggests that fungi also can produce nanoparticulate copper.

Some copper reduction possibly occurred in response to the European heat wave of the summer of 2003 (Supporting Information). Elevated expression of heat shock protein HSP90 and metallothionein genes has been observed in hyphae of an arbuscular mycorrhizal fungus in the presence of 2×10^{-5} M $CuSO_4$ in the laboratory (*52*). This suggests that a single driving force can trigger a biological defense mechanism that has multiple purposes. Thus, reduction of toxic cations to native elements may increase as rhizosphere biota fight metal stress and stresses imposed by elevated temperatures expected from global warming.

Reduction of Other Metal Cations to Their Metallic Forms. Laboratory evidence has shown that plants (*53–55*), fungi (*23, 56, 57*), bacteria (*58*), and algae (*59*) can transform other more easily reducible metals, including Au, Ag, Se (as H_2SeO_3), Hg, and Te, to their elemental states both intra- and extracellularly. When mechanisms have been proposed, they typically have involved enzymes; however, ascorbic acid was implicated when Hg^{2+} was transformed to Hg^0(g) in barley leaves (*60*). Theoretically all of these metal cations could be transformed by a reducing agent weaker than ascorbic acid (Table S1 in Supporting Information). However, binding appears to stabilize cationic forms in the absence of a sufficiently strong reductant such as ascorbic acid. Processes used in materials synthesis that were developed with biochemical knowledge might yield clues to other possible, but presently unknown, biologically mediated reactions in different organisms.

Natural Occurrence of Cu^0 and Environmental Implications. The discovery of nanoparticulate copper metal in phytoremediated soil may shed light on the occurrence of copper in peats. Native copper likely forms abiotically in the reducing acidic environments of Cu-rich peat bogs (*61*). However, swamps by definition are more oxidizing with neutral to alkaline pHs, and they may be ideal sites for biotic formation of metallic Cu nanoparticles. For example, in swamp peats near Sackville, New Brunswick, Canada, copper species unidentifiable by XRD were dissolved only with corrosive perchloric acid (*61*), suggesting they may have been nanoparticulate metal formed by active root systems of swamp plants. If swamp peats evolve to bog peats the Cu reduction mechanism could convert to autocatalysis on the

initial nanocrystals (*43*). The addition of peats that either act as templating substrates or contain nanoparticulate copper could enhance the effectiveness of using wetlands plants for phytoremediation. In contrast to harvesting hyperaccumulators, the oxygenated rhizosphere would become an economic source of biorecycled copper, and rhizosphere containment would prevent copper from entering the food chain via herbivores, limiting potential risks to humans.

Acknowledgments

The authors thank J. L. Hazemann (ESRF), O. Proux (ESRF), and S. Fakra (ALS) for assistance during EXAFS measurements and the ESRF and ALS for the provision of beamtime. The ALS is supported by the Director, Office of Energy Research, Office of Basic Energy Sciences, Materials Sciences Division of the U.S. Department of Energy, under Contract No. DE-AC02-05CH11231. Support was provided to A. Manceau from the ANR-ECCO program and to K. L. Nagy from U.S. National Science Foundation grant EAR-0447310.

Supporting Information Available

Additional information on the field site, and data interpretations, including thermodynamic calculations of Cu speciation in the soil solution. This material is available free of charge via the Internet at http://pubs.acs.org.

Literature Cited

(1) OJEC. On the quality of water intended for human consumption. *Off. J. Eur. Communities* **1998**, *L-330* (5 December 1998).
(2) EPA National primary drinking water standards. EPA Agency, 2003, EPA-816-F-03-016.
(3) EPA Aquatic life ambient freshwater quality criteria - copper 2007 revision. EPA Agency, EPA-822-F07-001.
(4) Vassilev, A.; Schwitzguébel, J. P.; Thewys, T.; Van der Lelie, D.; Vangronsveld, J. The use of plants for remediation of metal-contaminated soils. *Sci. World J.* **2004**, *4*, 9–34.
(5) MacFarlane, G. R.; Burchett, M. D. Cellular distribution of copper, lead and zinc in the grey mangrove, *Avicennia marina* (Forsk.) Vierh. *Aquat. Bot.* **2000**, *68*, 45–59.
(6) Van Hoof, N. A. L. M.; Hassinen, V. H.; Hakvoort, H. W. J.; Ballintijn, K. F.; Schat, H.; Verkleij, J. A. C.; Ernst, W. H. O.; Karenlampi, S. O.; Tervahauta, A. I. Enhanced copper tolerance in *Silene vulgaris* (Moench) Garcke populations from copper mines is associated with increased transcript levels of a 2b-type metallothionein gene. *Plant Physiol.* **2001**, *126*, 1519–1526.
(7) Clemens, S. Molecular mechanisms of plant metal tolerance and homeostasis. *Planta* **2001**, *212*, 475–486.
(8) Polette, L. A.; Gardea-Torresdey, J. L.; Chianelli, R. R.; George, G. N.; Pickering, I. J.; Arenas, J. XAS and microscopy studies of the uptake and bio-transformation of copper in *Larrea tridentate* (creosote bush). *Microchem. J.* **1998**, *65*, 227–236.
(9) Lidon, F. C.; Henriques, F. S. Subcellular localization of copper and partial isolation of copper proteins in roots from rice plants exposed to excess copper. *Aust. J. Plant Physiol.* **1994**, *21*, 427–436.
(10) Arru, L.; Rognoni, S.; Baroncini, M.; Bonatti, P. M.; Perata, P. Copper localization in *Cannabis sativa* L. grown in a copper-rich solution. *Euphytica* **2004**, *140*, 33–38.
(11) Liu, D.; Kottke, I. Subcellular localization of copper in the root cells of *Allium sativum* by electron energy loss spectroscopy (EELS). *Biores. Technol.* **2004**, *94*, 153–158.
(12) Ni, C. Y.; Chen, Y. X.; Lin, Q.; Tian, G. M. Subcellular localization of copper in tolerant and non-tolerant plant. *J. Environ. Sci. China* **2005**, *17*, 452–456.
(13) Hinsinger, P.; Gobran, G. R.; Gregory, P. J.; Wenzel, W. W. Rhizosphere geometry and heterogeneity arising from root-mediated physical and chemical processes. *New Phytol.* **2005**, *168*, 293–303.
(14) Manceau, A.; Marcus, M. A.; Tamura, N. Quantitative speciation of heavy metals in soils and sediments by synchrotron X-ray techniques. In *Applications of Synchrotron Radiation in Low-Temperature Geochemistry and Environmental Science*; Fenter, P. A., Rivers, M. L., Sturchio, N. C., Sutton, S. R., Eds.; Mineral. Soc. Amer.: Washington, DC, 2002; Vol. 49, pp 341–428.
(15) Weis, J. S.; Weis, P. Metal uptake, transport and release by wetland plants: Implications for phytoremediation and restoration. *Environ. Intern.* **2004**, *30*, 685–700.
(16) Peverly, J. H.; Surface, J. M.; Wang, T. Growth and trace metal absorption by *Phragmites australis* in wetlands constructed for landfill leachate treatment. *Ecol. Eng.* **1995**, *5*, 21–35.
(17) Stoltz, E.; Greger, M. Accumulation properties of As, Cd, Cu, Pb and Zn by four wetland plant species growing on submerged mine tailings. *Environ. Exp. Bot.* **2002**, *47*, 271–280.
(18) Deng, H.; Ye, Z. H.; Wong, M. H. Accumulation of lead, zinc, copper and cadmium by 12 wetland plant species thriving in metal-contaminated sites in China. *Environ. Pollut.* **2004**, *132*, 29–40.
(19) Kirpichtchikova, T.; Manceau, A.; Spadini, L.; Panfili, F.; Marcus, M. A.; Jacquet, T. Speciation and solubility of heavy metals in contaminated soil using X-ray microfluorescence, EXAFS spectroscopy, chemical extraction, and thermodynamic modelling. *Geochim. Cosmochim. Acta* **2006**, *70*, 2163–2190.
(20) Oliveira, R. S.; Dodd, J. C.; Castro, P. M. L. The mycorrhizal status of *Phragmites australis* in several polluted soils and sediments of an industrialised region of Northern Portugal. *Mycorrhiza* **2001**, *10*, 241–247.
(21) Leyval, C.; Turnau, K.; Haselwandter, K. Effect of heavy metal pollution on mycorrhizal colonization and function: physiological, ecological and applied aspects. *Mycorrhiza* **1997**, *7*, 139–153.
(22) Tonin, C.; Vandenkoornhuyse, P.; Joner, E. J.; Straczek, J.; Leyval, C. Assessment of arbuscular mycorrhizal fungi diversity in the rhizosphere of *Viola calaminaria* and effect of these fungi on heavy metal uptake by clover. *Mycorrhiza* **2001**, *10*, 161–168.
(23) Gadd, G. M. Geomycology: biogeochemical transformations of rocks, minerals, metals and radionuclides by fungi, bioweathering and bioremediation. *Mycol. Res.* **2007**, *111*, 3–49.
(24) Vesk, P. A.; Nockolds, C. E.; Allaway, W. G. Metal localization in water hyacinth roots from an urban wetland. *Plant, Cell Environ.* **1999**, *22*, 149–158.
(25) Panfili, F.; Manceau, A.; Sarret, G.; Spadini, L.; Kirpichtchikova, T.; Bert, V.; Laboudigue, A.; Marcus, M. A.; Ahamdach, N.; Libert, M. F. The effect of phytostabilization on Zn speciation in a dredged contaminated sediment using scanning electron microscopy, X-ray fluorescence, EXAFS spectroscopy and principal components analysis. *Geochim. Cosmochim. Acta* **2005**, *69*, 2265–2284.
(26) Manceau, A.; Marcus, M. A.; Tamura, N.; Proux, O.; Geoffroy, N.; Lanson, B. Natural speciation of Zn at the micrometer scale in a clayey soil using X-ray fluorescence, absorption, and diffraction. *Geochim. Cosmochim. Acta* **2004**, *68*, 2467–2483.
(27) Manceau, A.; Tommaseo, C.; Rihs, S.; Geoffroy, N.; Chateigner, D.; Schlegel, M.; Tisserand, D.; Marcus, M. A.; Tamura, N.; Chen, Z. S. Natural speciation of Mn, Ni and Zn at the micrometer scale in a clayey paddy soil using X-ray fluorescence, absorption, and diffraction. *Geochim. Cosmochim. Acta* **2005**, *69*, 4007–4034.
(28) Zabinsky, S. I.; Rehr, J. J.; Ankudinov, A.; Albers, R. C.; Eller, M. J. Multiple scattering calculations of X-ray absorption spectra. *Phys. Rev.* **1995**, *B52*, 2995–3009.
(29) Frenkel, A. I.; Hills, C. W.; Nuzzo, R. G. A view from the inside: Complexity in the atomic scale ordering of supported metal nanoparticles. *J. Phys. Chem.* **2001**, *105*, 12689–12703.
(30) DiCicco, A.; Berrettoni, M.; Stizza, S.; Bonetti, E.; Cocco, G. Microstructural defects in nanocrystalline iron probed by X-ray absorption spectroscopy. *Phys. Rev.* **1994**, *B50*, 12386–12397.
(31) Heaton, D. N.; George, G. N.; Garrison, G.; Winge, D. R. The mitochondrial copper metallochaperone cox17 exists as an oligomeric, polycopper complex. *Biochemistry* **2001**, *40*, 743–751.
(32) Otte, M. L.; Matthews, D. J.; Jacob, D. L.; Moran, B. M.; Baker, A. J. M. Biogeochemistry of metals in the rhizosphere of wetland plants. An explanation for 'innate' metal tolerance. In *Developments in Ecosystems*; Wong, M. H., Ed.; Elsevier: 2004.
(33) Battistuzzi, G.; Borsari, M.; Canters, G. W.; Loschi, L.; Righi, F.; Sola, M. Redox thermodynamics of blue copper proteins. *J. Am. Chem. Soc.* **1999**, *121*, 501–506.
(34) Schafer, F. Q.; Buettner, G. R. Redox environment of the cell as viewed through the redox state of the glutathione disulfide/glutathione couple. *Free Radical Biol. Med.* **2001**, *30*, 1191–1212.
(35) Huffman, D. L.; O'Halloran, T. V. Function, structure, and mechanism of intracellular copper trafficking proteins. *Annu. Rev. Biochem.* **2001**, *70*, 677–701.
(36) Buettner, G. R.; Jurkiewicz, B. A. Catalytic metals, ascorbate and free radicals: Combinations to avoid. *Radiat. Res.* **1996**, *145*, 532–541.
(37) Gadd, G. M. Interactions of fungi with toxic metals. *New Phytol.* **1993**, *124*, 25–60.
(38) Chisholm, J. E.; Jones, G. C.; Purvis, O. W. Hydrated copper oxalate, moolooite, in lichens. *Miner. Mag.* **1987**, *51*, 715–718.

(39) Lichtenegger, H. C.; Schoberl, T.; Bartl, M. H.; Waite, H.; Stucky, G. D. High abrasion resistance with sparse mineralization: copper biomineral in worm jaws. *Science* **2002**, *298*, 389–392.
(40) Slocik, J. M.; Wright, D. W. Biomimetic mineralization of noble metal nanoclusters. *Biomacromolecules* **2003**, *4*, 1135–1141.
(41) Song, J.; Zhao, F. J.; Luo, Y. M.; McGrath, S. P.; Zhang, H. Z. Copper uptake by *Elsholtzia spendens* and *Silene vulgaris* and assessment of copper phytoavailability in contaminated soils. *Environ. Pollut.* **2004**, *128*, 307–315.
(42) Monson, C. F.; Woolley, A. T. DNA-templated construction of copper nanowires. *Nano Lett.* **2003**, *3*, 359–363.
(43) Jana, N. R.; Wang, Z. L.; Sau, T. K.; Pal, T. Seed-mediated growth method to prepare cubic copper nanoparticles. *Curr. Sci.* **2000**, *79*, 1367–1370.
(44) Banerjee, I. A.; Yu, L.; Matsui, H. Cu nanocrystal growth on peptide nanotubes by biomineralization: Size control of Cu nanocrystals by tuning peptide conformation. *Proc. Natl. Acad. Sci.* **2003**, *1000*, 14678–14682.
(45) Horemans, N.; Foyer, C. H.; Potters, G.; Asard, H. Ascorbate function and associated transport systems in plants. *Plant Physiol. Biochem.* **2000**, *38*, 531–540.
(46) Hering, J. G.; Stumm, W. Oxidative and reductive dissolution of minerals. In *Mineral-Water Interface Geochemistry*; Hochella, M. F. J., White, A. F., Eds.; Mineral. Soc. Am.: 1990; Vol. 23, pp 427–465.
(47) Singh, S.; Saxena, R.; Pandey, K.; Bhatt, K.; Sinha, S. 2004 Response of antioxidants in sunflower (*Helianthus annuus* L.) grown on different amendments of tannery sludge: its metal accumulation potential. *Chemosphere* **2004**, *57*, 1663–1673.
(48) Meharg, A. A. The mechanistic basis of interactions between mycorrhizal associations and toxic metal cations. *Mycol. Res.* **2003**, *107*, 1253–1265.
(49) Bradley, R.; Burt, A. J.; Read, D. J. Mycorrhizal infection and resistance to heavy metal toxicity in *Calluna vulgaris*. *Nature* **1981**, *292*, 335–337.
(50) Schützendübel, A.; Polle, A. Plant responses to abiotic stresses: heavy metal-induced oxidative stress and protection by mycorrhization. *J. Exp. Bot.* **2002**, *53*, 1351–1365.
(51) Gonzalez-Chavez, C.; D'Haen, J.; Vangronsveld, J.; Dodd, J. C. Copper sorption and accumulation by the extraradical mycelium of different *Glomus spp.* (arbuscular mycorrhizal fungi) isolated from the same polluted soil. *Plant Soil* **2002**, *240*, 287–297.
(52) Hildebrandt, U.; Regvar, M.; Bothe, H. Arbuscular mycorrhiza and heavy metal tolerance. *Phytochemistry* **2007**, *68*, 139–146.
(53) Gardea-Torresdey, J. L.; Tiemann, K. J.; Parsons, J. G.; Gamez, G.; Herrera, I.; Jose-Yacaman, M. XAS investigations into the mechanism(s) of Au(III) binding and reduction by alfalfa biomass. *Microchem. J.* **2002**, *71*, 193–204.
(54) Gardea-Torresdey, J. L.; Parsons, J. G.; Gomez, E.; Peralta-Videa, J.; Troiani, H. E.; Santiago, P.; Yacaman, M. J. Formation and growth of Au nanoparticles inside live alfalfa plants. *Nano Lett.* **2002**, *4*, 397–401.
(55) Gardea-Torresdey, J. L.; Gomez, E.; Peralta-Videa, J. R.; Parsons, J. G.; Troiani, H. E.; Yacaman, M. J. Alfalfa sprouts: A natural source for the synthesis of silver nanoparticles. *Langmuir* **2003**, *19*, 1357–1361.
(56) Mukherjee, P.; Ahmad, A.; Mandal, D.; Senapati, S.; Sainkar, S. R.; Khan, M. I.; Parishcha, R.; Ajaykumar, P. V.; Alam, M.; Kumar, R.; Sastry, M. Fungus-mediated synthesis of silver nanoparticles and their immobilization in the mycelial matrix: A novel biological approach to nanoparticle synthesis. *Nano Lett.* **2001**, *1*, 515–519.
(57) Mukherjee, P.; Senapati, S.; Mandal, D.; Ahmad, A.; Khan, M. I.; Kumar, R.; Sastry, M. Extracellular synthesis of gold nanoparticles by the fungus *Fusarium oxysporum*. *Chem. Biol. Chem.* **2002**, *5*, 461–463.
(58) Southam, G.; Beveridge, T. J. The in vitro formation of placer gold by bacteria. *Geochim. Cosmochim. Acta* **1994**, *58*, 4527–4530.
(59) Greene, B.; Hosea, M.; McPherson, R.; Henzl, M.; Alexander, M. D.; Darnall, D. W. Interaction of gold(I) and gold(III) complexes with algal biomass. *Environ. Sci. Technol.* **1986**, *20*, 627–632.
(60) Battke, F.; Ernst, D.; Halbach, S. Ascorbate promotes emission of mercury vapour from plants. *Plant, Cell Environ.* **2005**, *28*, 1487–1495.
(61) Shotyk, W. Review of the inorganic geochemistry of peats and peatland waters. *Earth Sci. Rev.* **1988**, *25*, 95–176.
(62) Marcus, M. A.; MacDowell, A. A.; Celestre, R.; Manceau, A.; Miller, T.; Padmore, H. A.; Sublett, R. E. Beamline 10.3.2 at ALS: a hard X-ray microprobe for environmental and materials sciences. *J. Synchroton Radiat.* **2004**, *11*, 239–247.
(63) Proux, O.; Nassif, V.; Prat, A.; Ulrich, O.; Lahera, E.; Biquard, X.; Menthonnex, J. J.; Hazemann, J. L. Feedback system of a liquid-nitrogen-cooled double-crystal monochromator: design and performances. *J. Synchroton Radiat.* **2006**, *13*, 59–68.

ES072017O

Supporting information for

Formation of Metallic Copper Nanoparticles at the Soil-Root Interface

Alain Manceau[1], Kathryn L. Nagy[2], Matthew A. Marcus[3], Martine Lanson[1], Nicolas Geoffroy[1], Thierry Jacquet[4], Tatiana Kirpichtchikova[4]

[1]LGIT-Maison des Géosciences, CNRS and Université J. Fourier, 38041 Grenoble Cedex 9, France

[2]Department of Earth and Environmental Sciences, 845 West Taylor Street, MC-186, University of Illinois at Chicago, Chicago, Illinois 60607, USA

[3]Advanced Light Source, Lawrence Berkeley National Laboratory, One Cyclotron Road, Berkeley, CA 94720, USA

[4]Phytorestore—Site et Concept, Hôtel Vigée Le Brun, 8 rue du Sentier, 75002 Paris, France

Number of pages: 11

Number of Figures: 3

1- Field experiments

The phytoremediation experiment was conducted from May 2002 to September 2003 near Avrigny, France. Two holes 4 x 4 m^2 at the surface and 40 cm deep were dug in the ground, lined with a permeable membrane, and configured with basal drains to collect percolating irrigation waters. Soil aeration was achieved with a horizontal network of pipes at the depth of the liner connected to the surface by vertical pipes (capped to prevent ingress of precipitation) at 9 locations per pot. The two pots were filled with soil from the Pierrelaye plain (*1*), and vegetated with *Iris pseudoacorus* (Pot A) and *Phragmites australis* (Pot B). Initial concentrations of Zn, Pb, and Cu in the pot soil were 1103, 535, and 290 mg/kg, respectively. The two pots were exposed to natural precipitation and also irrigated. From May 2002 to early September 2003, the typical tri-weekly irrigation schedule for Pot A, expressed as amount of precipitation, was 100 mm (three times the average monthly precipitation) on the first day in week 1 and 6 mm per day for each of five consecutive days in week 2 and then again in week 3. From September 23 to October 14, 2002, Pot A was irrigated instead once per week with 25 mm of 0.05 M citrate (in water at pH 5.5) followed by flushing with 100 mm of water four days later. This removed about 20% of the initial Cu from Pot A as soluble copper-citrate complexes, which are not degraded easily by microbes (*2*), consistent with the higher effluent Cu concentrations observed (up to ~10^{-5} M in Pot A vs. ~ 10^{-7} M in Pot B). Pot B was watered with 100 mm on the first day of every week in anticipation of simulating periodic redox conditions expected during heavy rainfalls. However, thermodynamic calculations presented below show that Pot B remained dominantly in the stability field of Cu^{2+} species and rarely entered the stability field of Cu^{+} species which may be due to the aeration as well as a high flux rate of water through the soil. Neither pot was watered from July 7-21 in 2003. The European heat wave in the summer of 2003 (*3, 4*) extended from June through August, and the experimental site is located in a part of France in which air temperatures rose to their highest values (> 30 °C) in the first two weeks of August (*5*). However, temperatures declined to normal in the latter part of August, and the plants were still flourishing at the time of sampling in September 2003. At the end of the 16-month experiment, stems and leaves of *I. pseudoacorus* and *P. australis* contained only 0.14% and 0.03% of the initial soil Cu, respectively. Therefore, copper was accumulated only in root systems as expected for metal-tolerant plants.

2 - Association of Cu° with fungal hyphae in the rhizosphere of *I. pseudoacorus*

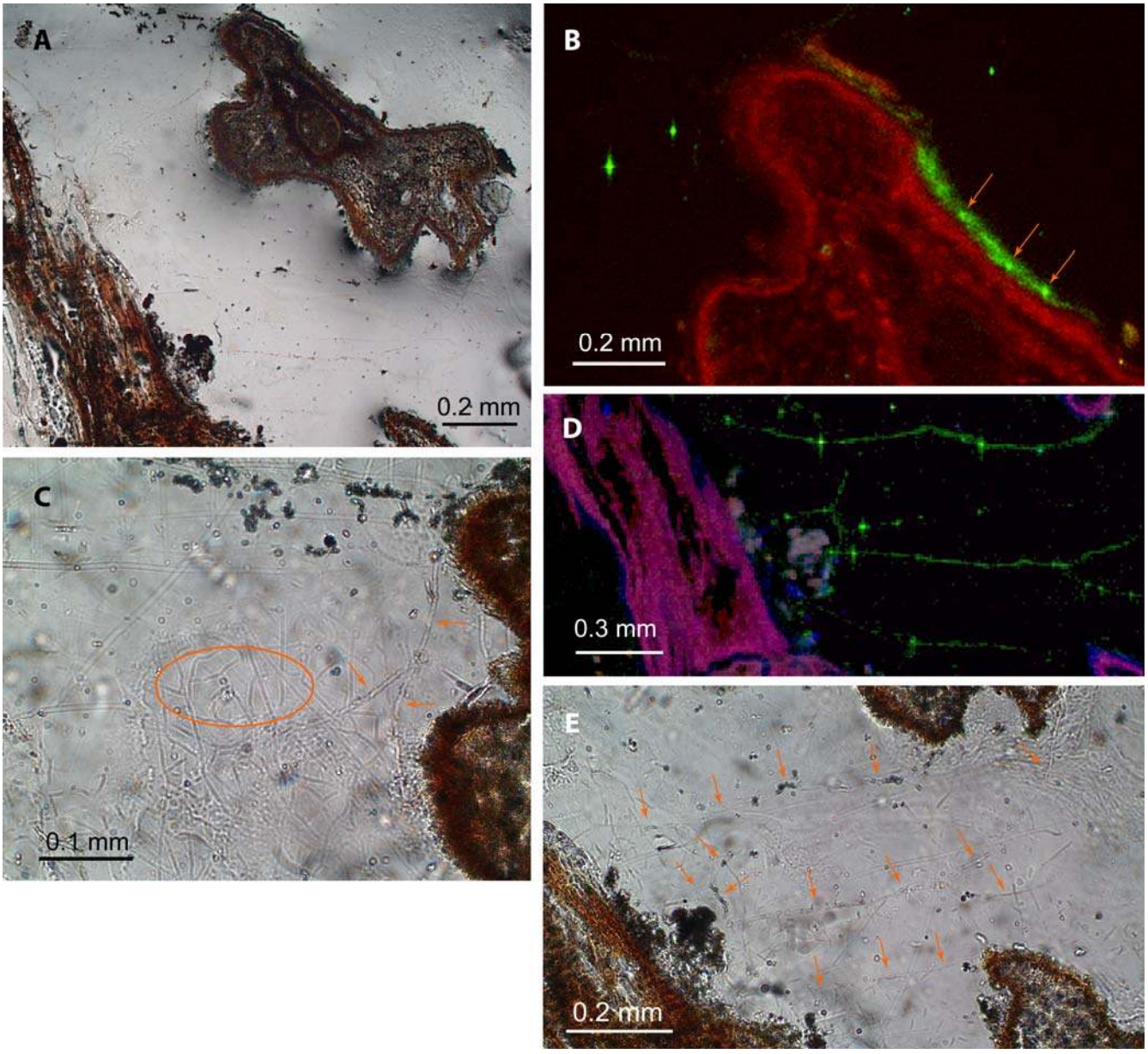

Fig. S1: (A) Longitudinal and transversal sections of roots from the rhizosphere of *I. pseudoacorus*. (**B**) Distribution of Zn (red) and Cu (green) in a layer at the surface of the root sectioned transversally in the optical micrograph S1A. The biofilm contains Cu(II) sorbed to organic matter (likely fungal hyphae) and Cu° grains pointed out with arrows. (**C**) Tangle of filamentous cells in the upper left region of S1A. Enlarging the image shows the presence of at least two kinds of filament morphologies (i.e., fungal species). (**D-E**) Fluorescence map and optical image of the lower region from S1A (Ca coded in blue). This close-up shows that the Cu° grains are aligned along the direction of fungal hyphae pointed out with arrows.

3 - Thermodynamic equilibria and redox potentials

Thermodynamic calculations using The Geochemist's Workbench (*6*), and assuming that effluent Cu concentrations represent uncomplexed or "free" copper ions, show that measured Eh-pH values straddled boundaries between the fields of dominance of Cu^{2+} and Cu^{+} species with no evidence that solutions entered the field of dominance of Cu^{0}, except intermittently in Pot A from May 5 to July 16, 2003 (Fig. S2A; Effluent solutions were not analyzed after July 16 for Pot A and after July 31 for Pot B). Dissolved copper would have been effectively completely bound to the dissolved organic carbon (DOC) (~ 10 mg/L on average in Pot B and 750 mg/L declining to ~130 mg/L in Pot A after citrate addition) based on binding constants for Cu to organic functional groups. Binding to DOC would have lowered the amount of free inorganic copper causing an increase in the dominance of aqueous copper species over solid species at the measured Eh-pH conditions of both pots, thus lessening even more the likelihood of abiotic precipitation of Cu^{0} in Pot A.

Starting in May 2003, the changes in Eh in Pot A positively correlated with the changes in pH, suggesting periodic triggering of one or more redox reactions (Fig. S2B). The correlation began well before the peak of the heat wave in 2003 and was not observed in Pot B. Because Pot A received less water, its soil may have begun to dry increasing dissolved copper and hydroxyl concentrations and initiating enhanced plant and/or fungal defenses against the higher copper concentrations. Increased biological production of one or more active reducing agents would simultaneously lower pH and Eh, and thus precipitate copper metal. Subsequent watering would have reduced the oxidative stress bringing the system back to higher pH and Eh values. These Eh-pH changes also might be related to a shift in community balance between arbuscular mycorrhizal fungi, expected in alkaline environments (*7*), and ericoid mycorrhizal fungi, known to inhabit metal-contaminated acidic environments (*8, 9*) and to impart copper resistance to plants (*10*). Other biological processes could change pH, but not Eh simultaneously including for example, enhanced production by endomycorrhizal fungi of organic (citric and/or oxalic (*11*)) acids used to complex and precipitate excess Cu or bacterial decomposition of organic matter to produce CO_2. Thus, only a biotically mediated redox reaction is indicated by the Eh-pH data, while a direct causative effect of higher air temperatures is inconclusive.

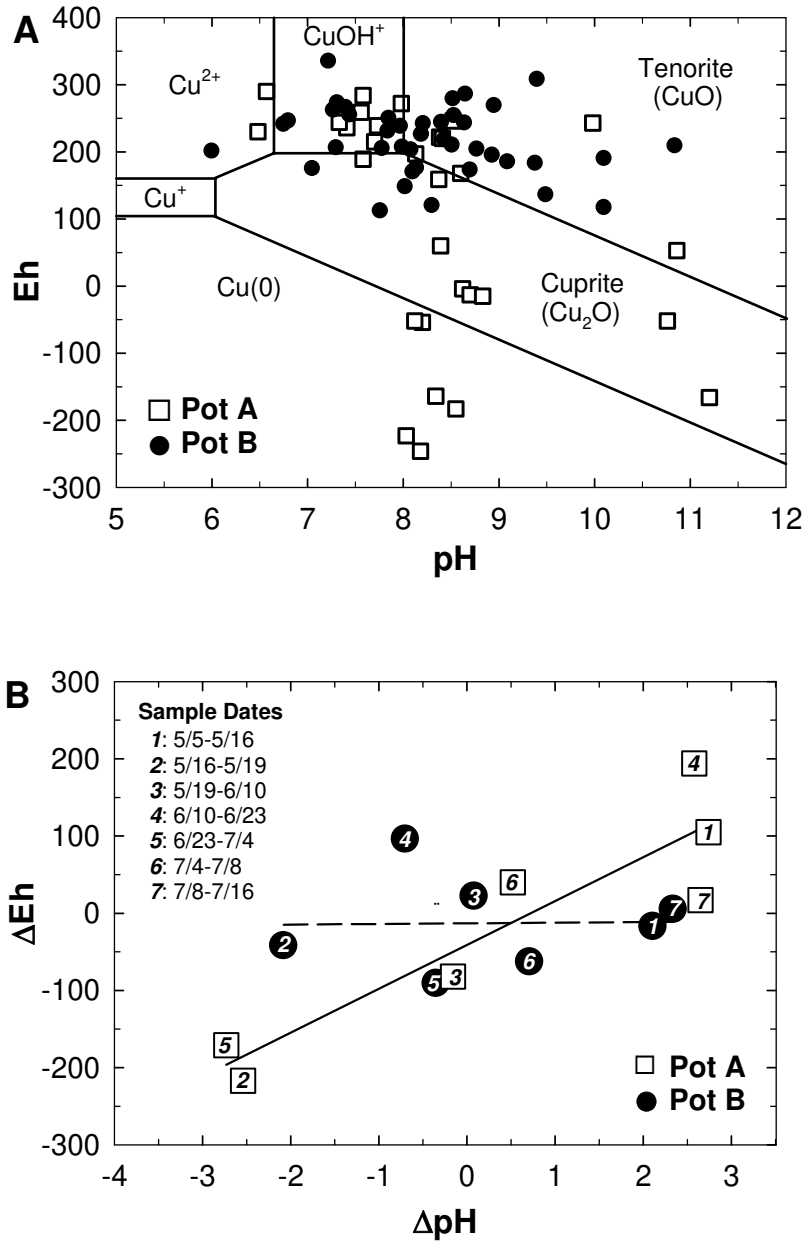

Fig. S2: (**A**) Eh-pH diagram for a 25 °C solid-aqueous system with 10^{-7} M dissolved Cu showing fields of dominance of Cu species and measured parameters in pot effluents. Fields of dominance for Cu^+ aqueous species enlarge slightly at 35 °C and shrink slightly at 5 °C for $[Cu(aq)_{total}] = 10^{-7}$ M, and disappear completely at 5-35 °C for $[Cu(aq)_{total}] = 10^{-5}$ M. Fields of dominance for all solid phases shift to higher pH and lower Eh as $[Cu(aq)_{total}] \rightarrow 0$. (**B**) Change in Eh vs. change in pH for pot solutions from May 5 to July 16, 2003. Data from Pot B are uncorrelated ($r^2 = 4.3 \times 10^{-4}$), but data from Pot A are correlated linearly with a slope of 56.8, intercept of -41.1 mV at $\Delta pH = 0$ and $r^2 = 0.835$, suggesting that the changes are driven by one or more redox reactions in Pot A.

We proposed that biotic ascorbic acid production would drive the reduction of toxic copper cations. The half cell potential of the dehydroascorbate/ascorbic acid couple is lower than those for any copper couples and therefore ascorbic acid theoretically could reduce cationic copper (Table S1).

However, this reduction cannot occur in a solution of free copper cations (*12*) and appears to be facilitated only in the presence of a templating substrate (*13, 14*), such as fungal hyphae (Fig. S1B). Additionally, the cellular redox environment is regulated by multiple reactions many of which involve radical intermediates, including the ascorbate radical (*15-17*). Thus, although increased production of ascorbic acid by rhizosphere biota is proposed here as the key step in the reduction mechanism, the situation may be more complex, as outlined for Hg^{2+} reduction to Hg^0 in barley (*18*).

Table S1.Redox potentials of reducible metals by biota and ascorbic acid

Half-reaction[1]	**E^0, Standard Electrode Potential (V)**[2]
$Au^+ + e^- = Au(s)$	1.83
$Au^{3+} + 3e^- = Au(s)$	1.52
$Ag^+ + e^- = Ag(s)$	0.80
$Hg^{2+} + 2e^- = 2Hg(l)$	0.80
$H_2SeO_3(aq) + 4H^+ + 4e^- = Se(s) + 3H_2O$	0.74
$Te^{4+} + 4e^- = Te(s)$	0.57
$Cu^+ + e^- = Cu(s)$	0.52
$Cu^{2+} + 2e^- = Cu(s)$	0.34
$2Cu^+ = Cu(s) + Cu^{2+}$	0.18
[3]DHAA + 2e- + $2H^+$ = AA	0.08

[1]Cations in all half-reactions are aqueous species. Note that certain half reactions are pH-dependent.
[2]Half-cell potentials from (*19, 20*).
[3]Dehydroascorbate-ascorbic acid reaction can involve intermediate ascorbate radical forms, not shown here (*15-17*).

4- Cu speciation in the rhizosphere

Initial soil. The binding mechanism of Cu in the initial soil was determined by comparing the unknown spectra with those from a large database of spectral references, including Cu complexed to low molecular-weight aqueous organic acids (acetate, citrate) and to humic acids from the Elliott soil and Florida peat of the International Humic Substances Society (IHSS). In all cases, Cu was observed to be bound to carboxylic functional groups, as described in the literature (*21-26*).

Nature of Cu nanocrystals in the phytoremediated soil. The only change in copper speciation was the appearance of the Cu^0 metallic species. No evidence was seen for the formation of other rarely-reported copper biominerals which all contain Cu^+ or Cu^{2+}: copper-sulfide (*27*), copper oxalate (*11, 28*), or atacamite (*29*).

Data were simulated with the FEFF 7.01 code (*30*). Structural parameters were determined by Fourier-filtering the data in real space over the [1.4 - 5.4 Å] $R+\Delta R$ interval, and least-squares fitting the filtered spectrum over the [3.0 - 12.4 $Å^{-1}$] k interval. Contributions from multiple-scattering paths were added to the fits, and metallic Cu was used as reference for calibrating the many-body amplitude reduction factor S_0^2, and verifying the correctness of the mean-free path of the electron λ, and the amplitude and phase shift functions.

Proportion of Cu bound to organics in the Cu nanocrystals. The radial structure function of the μ-EXAFS spectrum for the Cu organic species has a prominent peak at $R+\Delta R$ = 1.5 Å, assigned to the Cu-O pair at R = 1.94 Å (Fig. S3). If 40 % of the Cu organic signal is added to 100% of the EXAFS signal for the Cu grains, and the composite spectrum is Fourier transformed, the organic component, now at 29% of the total signal, manifests itself in the appearance of a shoulder on the left side of the Cu-Cu peak. The imaginary part of the Fourier transform has a minimum at $R+\Delta R$ = 1.35 Å, and otherwise oscillates about $y = 0$ in the absence of Cu-O pairs. Thus, the maximum fraction of Cu bound to organics needed to bring the curve representing the mixture to within the precision of the Fourier transform for the Cu grains (i.e., a distance midway between the curves for the Cu grains and mixture of Cu grains + Cu-organics) is estimated to be 15 %. This simulation also shows that EXAFS has a high sensitivity to multi-atom Cu^0 clusters, because the signal from the C shells for the Cu organic component is weak in comparison to that from the Cu shells.

Proportion of Cu^0 in the remediated soils. The bulk EXAFS spectra were recorded at 10 K, whereas μ-EXAFS spectra can be recorded only at room temperature with current instrumentation at synchrotron facilities. The proportions of each Cu species were bracketed by decomposing the bulk spectra alternately with that of massive Cu metal at 10 K (lower bound) and that of the Cu nanoparticle aggregates at room temperature (upper bound).

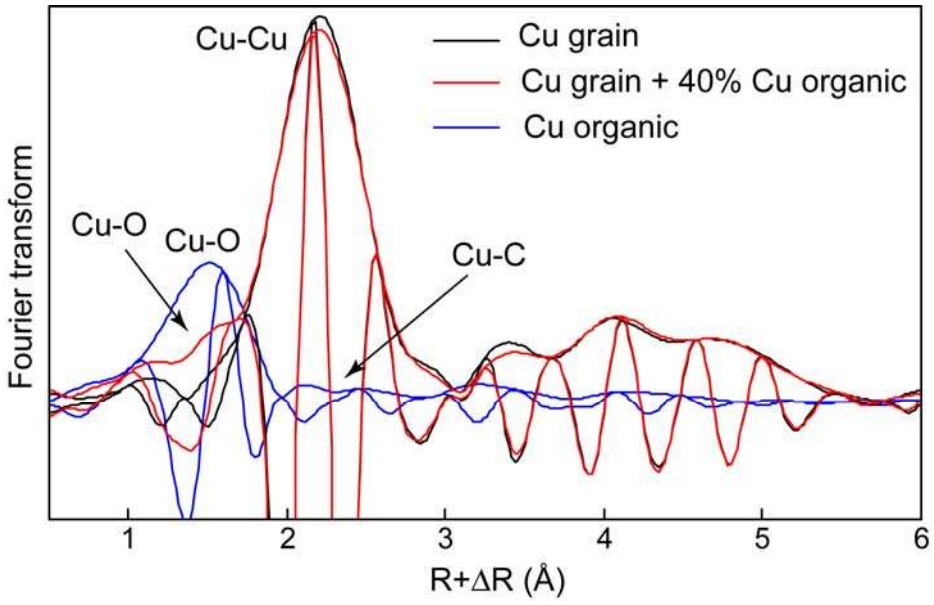

Fig. S3: Fourier transforms (modulus plus imaginary part) of the μ-EXAFS spectra from Figure 2A (Cu organic) and 2B (Cu grain), and from the composite spectrum corresponding to a mixture of 100% Cu grain + 40% Cu organic.

5- Detection of Cu^0 crystallites by XRD

The presence of a visible diffraction ring on the XRD patterns of some Cu grains indicates that these spots contain crystallized Cu^0 particles. Diffraction sees preferentially the largest particles, while EXAFS sees every atom in every particle equally. Thus, we need to know what proportion of Cu atoms is in the diffracting crystallites. In order to demonstrate how many crystallites are required to produce a smooth powder ring, we simulated the diffraction from a set of randomly oriented particles. Each crystallite was considered to produce diffraction intensity centered around each of the eight equivalent reflections produced by the {111} planes of metallic copper. For particles of radius *r*, the diffracted intensity was described as:

$$I_p(q) = \begin{cases} \exp(-(qr)^2/5) & qr \le q_0 \\ 9/(2q^4r^4) & qr > q_0 \end{cases}$$

where $q_0 = 4.9440$ Å^{-1} is chosen to make this function continuous and $q = \left|\vec{q}_{scatt} - \vec{g}_{hkl}\right|$. Here, $\vec{q}_{scatt}$ is the scattering wavevector and $\vec{g}_{hkl}$ is the Bragg vector for the *hkl* reflection. This form was chosen to have the correct Guinier and Porod limits for a spherical particle, but not the oscillations seen in the exact form. This assumed form allows for polydispersity and non-spherical shapes. We then rotated the crystallites about random axes by random amounts, and for each crystallite calculated the diffracted

intensity at various angles along the Debye ring. Adding up the contributions for all reflections from all crystallites yields the simulated powder pattern. We then adjusted the number of crystallites to yield a "smooth" diffraction ring as defined by a standard deviation of intensity along the ring equal to 10% of the mean.

This calculation also produces a version of the Debye formula relating domain size to peak width. By performing an angular integration on our assumed peak shape, we find that the domain radius is given by $r = 0.6dq_{\max} / \Delta q$, where d is the *d*-spacing, $q_{\max}$ is the wave vector of the peak, and Δq is the FWHM (Full Width at Half Maximum) of the peak. The result is that about 250,000 crystallites are required to produce a smooth ring for an effective diameter (2*r*) of the diffracting crystallites of 140 Å on average. Each crystallite has a volume of about 1.4 10^{-6} μm^3, so the minimum volume of diffracting particles in the beam is about 0.36 μm^3. For a probe volume of 16 x 7 x 30 μm^3, the crystallite volume fraction is 1.1 10^{-4}, and the column density of Cu is equivalent to a metallic Cu foil with an effective thickness of about 32 Å. Since this amount of Cu is unlikely to produce as strong a fluorescence signal as we see in EXAFS and XRF, most of the Cu^0 in the diffracting spots must be nanoparticles which do not diffract effectively.

5- Literature cited

(1) Kirpichtchikova, T.; Manceau, A.; Spadini, L.; Panfili, F.; Marcus, M. A.; Jacquet, T. Speciation and solubility of heavy metals in contaminated soil using X-ray microfluorescence, EXAFS spectroscopy, chemical extraction, and thermodynamic modelling. *Geochim. Cosmochim. Acta* **2006**, *70*, 2163-2190.

(2) Francis, A. J.; Dodge, C. J.; Gillow, J. B. Biodegradation of metal citrate complexes and implications for toxic-metal mobility. *Nature* **1992**, *356*, 140-142.

(3) Beniston, M. The 2003 heat wave in Europe: A shape of things to come? An analysis based on Swiss climatological data and model simulations. *Geophys. Res. Lett.* **2004**, *31*, L02202.

(4) Schär, C.; Vidale, P. L.; Lüthi, D.; Frei, C.; Häberli, C.; Liniger, M. A.; Appenzeller, C. The role of increasing temperature variability in European summer heatwaves. *Nature* **2004**, *427*, 332-336.

(5) NASA, http://visibleearth.nasa.gov/view_rec.php?id=16544 (2007).

(6) Bethke, C. M. *The Geochemist's Workbench®-v. 4.0*. University of Illinois 2002.

(7) Meharg, A. A. The mechanistic basis of interactions between mycorrhizal associations and toxic metal cations. *Mycol. Res*. **2003**, *107*, 1253-1265.

(8) Cairney, J. W. G.; Meharg, A. A. Influences of anthropogenic pollution on mycorrhizal fungal communities. *Environ. Poll.* **1999**, *106*, 169-182.

(9) Cairney, J. W. G.; Meharg, A. A. Ericoid mycorrhiza: a partnership that exploits harsh edaphic conditions. *Eur. J. Soil Sci.* **2003**, *54*, 735.740.

(10) Bradley, R.; Burt, A. J.; Read, D. J. Mycorrhizal infection and resistance to heavy metal toxicity in *Calluna vulgaris*. *Nature* **1981**, *292*, 335-337.

(11) Gadd, G. M. Geomycology: biogeochemical transformations of rocks, minerals, metals and radionuclides by fungi, bioweathering and bioremediation. *Mycol. Res.* **2007**, *111*, 3-49.

(12) Jana, N. R.; Wang, Z. L.; Sau, T. K.; Pal, T. Seed-mediated growth method to prepare cubic copper nanoparticles. *Curr. Sci*. **2000**, *79*, 1367-1370.

(13) Slocik, J. M.; Moore, J. T.; Wright, D. W. Monoclonal antibody recognition of histidine-rich peptide encapsulated nanoclusters. *Nano Lett.* **2002**, *2*, 169-173.

(14) Slocik, J. M.; Wright, D. W. Biomimetic mineralization of noble metal nanoclusters. *Biomacromol.* **2003**, *4*, 1135-1141.

(15) Buettner, G. R. The pecking order of free radicals and antioxidants: Lipid peroxidation, α-tocopherol, and ascorbate. *Arch. Biochem. Biophys*. **1993**, *300*, 535-543.

(16) Buettner, G. R.; Jurkiewicz, B. A. Catalytic metals, ascorbate and free radicals: Combinations to avoid. *Rad. Res.* **1996**, *145*, 532-541.

(17) Schafer, F. Q.; Buettner, G. R. Redox environment of the cell as viewed through the redox state of the glutathione disulfide/glutathione couple. *Free Rad. Biol. Med.* **2001**, *30*, 1191-1212.

(18) Battke, F.; Ernst, D.; Halbach, S. Ascorbate promotes emission of mercury vapour from plants. *Plant Cell Environ.* **2005**, *28*, 1487-1495.

(19) White, A.; Handler, P.; Smith, E. L. *Principles of Biochemistry*, 5th ed. New York, McGraw-Hill: 1973; p 1295.

(20) Bard, A. J.; Parsons, R.; Jordan, J. *Standard Potentials in Aqueous Solutions*. IUPAC (Marcel Dekker), New York, USA,: 1985.

(21) Hesterberg, D.; Sayers, D. E.; Zhou, W.; Robarge, W. P.; Plummer, G. M. XAFS characterization of copper in model aqueous systems of humic acid and illite. *J Phys IV* **1997**, *7*, 833-834.

(22) Xia, K.; Bleam, W.; Helmke, P. A. Studies of the nature of Cu^{2+} and Pb^{2+} binding sites in soil humic substances using X-ray absorption spectroscopy. *Geochim. Cosmochim. Acta* **1997**, *61*, 2211-2221.

(23) Xia, K.; Bleam, W.; Helmke, P. A. Studies of the nature of binding sites of first row transition elements bound to aquatic and soil humic substances using X-ray absorption spectroscopy. *Geochim. Cosmochim. Acta* **1997**, *61*, 2223-2235.

(24) Korshin, G. V.; Frenkel, A. I.; Stern, E. A. EXAFS study of the inner shell structure in copper(II) complexes with humic substances. *Environ. Sci. Technol.* **1998**, *32*, 2699-2705.

(25) Frenkel, A. I.; Korshin, G. V. Studies of Cu(II) in soil by X-ray absorption spectroscopy. *Canad. J. Soil Sci.* **2001**, *81*, 271-276.

(26) Alcacio, T. E.; Hesterberg, D.; Chou, J. W.; Martin, J. D.; Beauchemin, S.; Sayers, D. E. Molecular scale characteristics of Cu(II) bonding in goethite-humate complexes. *Geochim. Cosmochim. Acta* **2001**, *65*, 1355-1366.

(27) Gadd, G. M. Interactions of fungi with toxic metals. *New Phytol.* **1993**, *124*, 25-60.

(28) Chisholm, J. E.; Jones, G. C.; Purvis, O. W. Hydrated copper oxalate, moolooite, in lichens. *Miner. Mag*. **1987**, *51*, 715-718.

(29) Lichtenegger, H. C.; Schoberl, T.; Bartl, M. H.; Waite, H.; Stucky, G. D. High abrasion resistance with sparse mineralization: copper biomineral in worm jaws. *Science* **2002**, *298*, 389-392.

(30) Ankudinov, A. L.; Ravel, B.; Rehr, J. J.; Conradson, S. D. Real space multiple scattering calculation of XANES. *Phys. Rev.* **1998**, *B58*, 7565-7576.